Quantifying tissue microvasculature with speckle variance optical coherence tomography

Leigh Conroy,[1] Ralph S. DaCosta,[1,2] and I. Alex Vitkin[1,2,*]

[1]*Department of Medical Biophysics, University of Toronto, Toronto, Ontario M5G 2M9, Canada*

[2]*Ontario Cancer Institute, University Health Network, Toronto, Ontario M5G 2M9, Canada*

**Corresponding author: Alex.Vitkin@rmp.uhn.on.ca*

Received May 15, 2012; accepted June 8, 2012;
posted June 27, 2012 (Doc. ID 167793); published July 25, 2012

In this Letter, we demonstrate high resolution, three-dimensional optical imaging of *in vivo* blood vessel networks using speckle variance optical coherence tomography, and the quantification of these images through the development of biologically relevant metrics using image processing and segmentation techniques. Extracted three-dimensional metrics include vascular density, vessel tortuosity, vascular network fractal dimension, and tissue vascularity. We demonstrate the ability of this quantitative imaging approach to characterize normal and tumor vascular networks in a preclinical animal model and the potential for quantitative, longitudinal vascular treatment response monitoring.

OCIS codes: 110.4500, 170.3880, 100.2000, 100.2960, 170.6935.

Tumors require access to blood vessels for oxygen and nutrient exchange, making the tumor vasculature an attractive potential target for cancer therapies. Tumor vasculature is poorly organized, leaky, and tortuous, often resulting in poorly oxygenated (hypoxic) tissue regions that are resistant to most cancer treatments, including chemotherapy and radiation therapy [1]. Recently, the role of tumor vasculature has been gaining increasing attention as a potential biomarker and therapeutic target in cancer treatment [2]. Optical modalities that have been used for preclinical vascular imaging include fluorescence microscopy, hyperspectral imaging, and optical coherence tomography (OCT) (see [3] for a recent review). Speckle variance OCT (svOCT), a functional extension of traditional OCT, can yield direct and depth-resolved visualization of vessels as small as ~15–25 μm in diameter without the use of contrast agents. However, these detailed and complex three-dimensional (3D) vascular images are difficult to assess by *qualitative* observation, and vascular changes in response to treatment are often too subtle to detect by the unaided eye. *Quantitative* longitudinal *in vivo* monitoring of tumor vascular structure will provide greater insight into the underlying vascular contributions to disease progression and treatment response. Here, we demonstrate the development of vascular metrics from svOCT images for quantitative vascular imaging *in vivo*.

svOCT provides depth-resolved, high-resolution visualization of vasculature *in vivo*; unlike Doppler imaging, speckle variance is independent of blood flow or imaging angle [4]. 3D vascular images are obtained by calculating the interframe variance (SV_{ijk}) of N consecutive B-mode OCT structural intensity (I_{ijk}) images pixel-by-pixel within the sample, where N is the number of frames used in the variance calculation (gate length) [4]:

$$\mathrm{SV}_{ijk} = \frac{1}{N}\sum_{n=1}^{N}\left(I_{ijkn} - \frac{1}{N}\sum_{n=1}^{N} I_{ijkn}\right)^2. \quad (1)$$

Vascular (fluid) regions decorrelate faster than solid tissue, and this difference in the time-varying properties of fluids and solids gives rise to different speckle patterns, yielding endogenous contrast between blood-filled vessels and surrounding tissues. Because the contrast is derived from inherent tissue properties, unlike fluorescence microscopy, svOCT does not require the use of exogenous contrast agents.

The OCT system has been described previously [5]. Briefly, images were acquired with a 36 kHz Fourier domain mode-locked swept source OCT system with a fiber ring laser consisting of a polygon-based tunable filter with a 110 nm sweeping range centered at 1310 nm and an average optical output power of 48 mW. The system resolutions in tissue were ~8 μm axially and ~13 μm laterally. Vessels smaller than the lateral resolution of the system cannot be resolved and therefore were not included in the quantification.

A dorsal skin fold window chamber (DSWC) model, shown in Fig. 1(a), was used in nude mice for direct

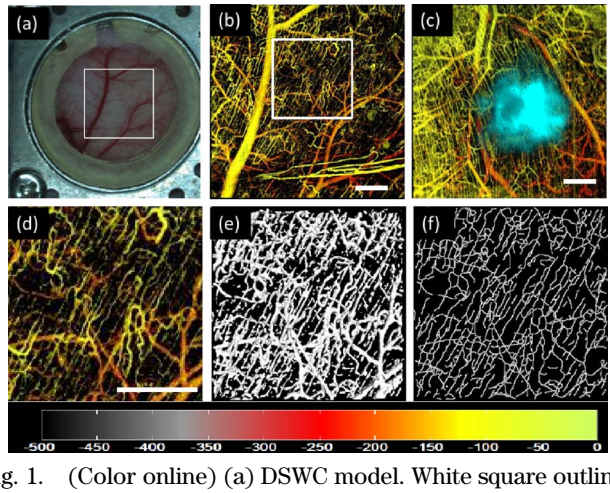

Fig. 1. (Color online) (a) DSWC model. White square outlines svOCT image area in (b). (b) svOCT image of *in vivo* normal vasculature. svOCT images are color-depth encoded, color bar represents vessel depth in tissue from the coverslip in μm. White box outlines region of interest (ROI) in (d), (e), and (f). (c) svOCT image of tumor vasculature overlaid with fluorescent ME180 tumor cells (cyan). (d) Normal ROI from (b). (e) 3D binary isosurface rendering of (d). (f) 3D isosurface representation of the 3D skeleton of (d). Scale bars 1 mm.

microscopic visualization of vasculature in normal and tumor tissue. Six mice were used to test the derived svOCT metrics comparing normal ($n = 3$) and tumor ($n = 3$) vasculature. To minimize bulk tissue motion artifacts, anaesthetized mice were restrained using a customized holder during imaging. For tumor-bearing mice, ME180 human cervical carcinoma cells transfected with the DsRed2 fluorescent protein were injected into the fascia and grown for one week before imaging. The fluorescent protein enabled tumor cell visualization and subsequent coregistration of fluorescent and svOCT images. All animal procedures were performed under ketamine-xylazine anaesthetic and approved by the University Health Network Animal Resource Centre.

Normal and tumor-bearing mice were imaged *in vivo* using svOCT over a 6×6 mm^2 field of view with 800 A-scans per frame and a gate length of $N = 8$. We have previously shown that this gate length is optimal for low bulk tissue motion scenarios, such as the DSWC [5]. 3D speckle variance images were averaged in the axial and lateral (B-scan) directions to produce an isotropic voxel size of ~ 8 μm^3. The forward scattering of photons by red blood cells results in shadowing artifacts below blood vessels; these artifacts were minimized by applying a step-down exponential filter in the axial direction, attenuating underlying voxels by a numerical factor proportional to the sum of the voxels immediately above [6]. A two-dimensional (2D) median filter with a window size of 3×3 pixels was applied to speckle variance images in each axial plane in the z direction to reduce "salt and pepper noise", and a hard threshold was applied to truncate low-intensity noise. In tumor-bearing mice, vascular quantification was performed over regions of interest encompassing the tumor as defined by the DsRed2 fluorescence image overlaid on the projected svOCT image, and in similarly located regions in non-tumor-bearing mice [Figs. 1(b) and 1(c)].

Following the image postprocessing described above, svOCT images were converted to 3D skeletons to facilitate analysis of the vascular networks. Skeletonization reduces each vessel to its median line, retaining its fundamental topology, orientation, and connectivity at the expense of losing vessel diameter information. For 3D skeletonization of svOCT images, an algorithm that alternated between object thinning and pruning was used [7] [Fig. 1(f)]. The pruning algorithm removed small surface features; this reduced vessel artefacts resulting from image noise and vessel-surface irregularities. The algorithm is fully described and validated elsewhere [7] and available as freeware [8].

Quantitative vascular metrics were derived from extracted skeletons using MATLAB (The MathWorks, Natick, Massachusetts) and ImageJ (National Institutes of Health, Bethesda, Maryland). Four metrics were extracted directly from the 3D skeletal images: (1) vessel segment density (VSD), (2) vascular length density (VLD), (3) average vascular tortuosity, and (4) fractal dimension. Figure 2 presents these analyses; note that for each of the four derived metrics, the difference between the tumor and normal values exceeds the intra-animal variation in the two groups.

The number of vessel segments in the volume of interest was calculated in ImageJ, where a vessel segment

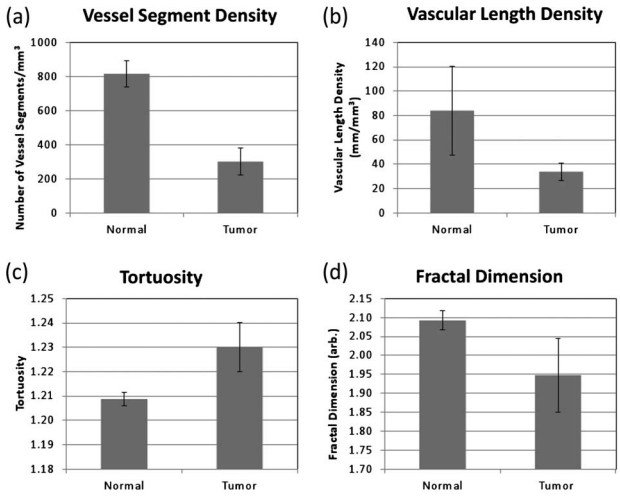

Fig. 2. Quantitative results comparing tumor and normal vascular characteristics for the four different metrics derived from 3D skeletonization of svOCT images ($n = 3$ animals for each group). Error bars represent standard deviation between mice.

was defined as any line connecting a branch point and an end point, or two branch points. This number was divided by the volume of the analyzed region to obtain VSD. The average VSD of normal vasculature was higher than that of tumor vasculature [Fig. 2(a)]. This can be explained by the presence of large avascular regions within the tumors. The volumetric VLD is an alternate microvascular metric that provides information complementary to VSD [Fig. 2(b)]. It is computed by dividing the sum of the vessel lengths by the interrogated volume. Together, VLD and VSD describe 3D microvascular density, a 2D measurement used in histology to assess tumor angiogenesis [9].

The tortuosity of each vessel segment was computed by dividing the length of the segment by the straight line Euclidean distance between its end points. The average tortuosity of the vessels within the volume was computed from the mean of these values. The minimum value of tortuosity is 1, indicating a straight vessel; as tortuosity increases, the efficiency of blood transport through the vessels decreases. Biologically, increased vascular tortuosity is indicative of disease, and can be related to vascular dysfunction [10]. As predicted in the literature using qualitative observations [11], the quantified average tortuosity of the tumor vasculature in our study was slightly higher than that of the normal [$\sim$1.23 versus $\sim$1.21, Fig. 2(c)].

Fractal dimension is a statistical measure used to characterize the degree of space filling of a vascular network. Biologically, this measurement can reflect the efficiency of oxygen and nutrient delivery to the tissue by quantifying the vascular network complexity [12]. Fractal dimensions for normal and tumor vascular networks were extracted using a 3D box-counting algorithm applied to the 3D vascular skeletons [13]. The fractal dimension was acquired by decreasing the cube size of a 3D grid overlaid on the skeleton and counting the number of filled cubes at each scale. The natural logarithm of the number of filled cubes was then plotted against the natural logarithm of the cube side length, and the fractal dimension was the slope of the linear portion of this plot.

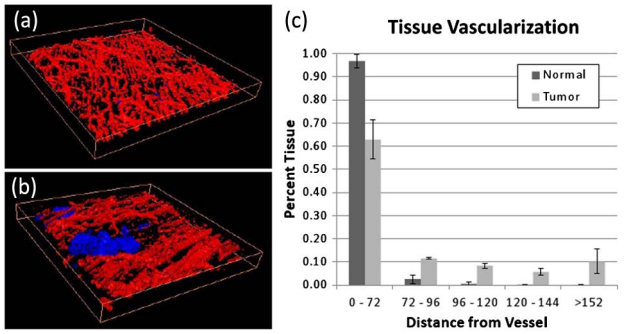

Fig. 3. (Color online) Isosurface rendering of 3D svOCT image (red = vessels) and areas of tissue more than 100 μm from any vessel in 3D (blue = potential hypoxic tissue) for (a) normal and (b) tumor vasculature. (ROI = 2.4 mm× 2.4 mm × 0.5 mm) (c) Comparison of normal ($n = 3$) and tumor ($n = 3$) tissue vascularization distribution; error bars represent standard deviation of histogram values between mice.

The fractal dimension of the normal vasculature was higher than the tumor [~2.09 versus ~1.95, where 3.0 would indicate a completely filled volume, Fig. 2(d)]. This suggests that normal vasculature is overall more space-filling than tumor networks, which are spatially heterogeneous with highly avascular as well as densely vascular regions [cf. discussion of Fig. 2(a)]. In future, use of smaller regions of interest to assess this vascular heterogeneity will be explored.

Qualitative evaluation of extracted vessels showed good agreement with original images; however, it was noted that the skeletonization can be sensitive to image noise and vessel surface irregularities. Consequently, metric values are somewhat dependent on original image quality; image preprocessing and skeleton pruning were used to reduce artefacts. Additional studies (independent validation, intermediate pathology grades, additional time points, and more animals) are required for optimization and validation of robustness and reproducibility of this approach.

All tissues require oxygen, and cells that are beyond the average oxygen diffusion distance (~100 μm) from a vessel are likely to be hypoxic and/or treatment resistant [14]. To quantify this, the 3D Euclidean distance transform was computed from a 3D binary vascular map [Fig. 1(e)]; each value yielded the distance between that point and the nearest vessel. The resultant 3D image can be used to visually identify tumor regions that are likely to be hypoxic [Figs. 3(a) and 3(b)]. Furthermore, tissue vascularization can be quantified by plotting the distance transform distribution histogram [Fig. 3(c)]. This metric intrinsically includes information about vessel diameter, a potentially important quantity that is lost in the skeleton-derived metrics.

In summary, we have developed quantitative metrics that uncover and measure vascular characteristics from 3D svOCT images. Our approach enabled *in vivo* characterization of normal and tumor microvasculature imaged within the DSWC model. Each metric provides a unique description of a particular microvascular characteristic and in combination with others offers quantitative insight into the underlying biology of vascular development and response. In the future, this methodological platform will be used preclinically for studying longitudinal vascular effects of cancer treatments such as radiation therapy and antivascular drugs.

This research was supported by the Natural Sciences and Engineering Research Council of Canada and Canadian Institutes of Health Research. Helpful discussions with Dr. John Sled, Dr. Adrian Mariampillai, and Azusa Maeda are gratefully acknowledged.

References

1. R. K. Jain, Nat. Med. **7**, 987 (2001).
2. D. W. Siemann and M. R. Horsman, Cell Tissue Res. **335**, 241 (2009).
3. S. J. Lunt, C. Gray, C. C. Reyes-Aldasoro, S. J. Matcher, and G. M. Tozer, J. Biomed. Opt. **15**, 011113 (2010).
4. A. Mariampillai, B. A. Standish, E. H. Moriyama, M. Khurana, N. R. Munce, M. K. K. Leung, J. Jiang, A. Cable, B. C. Wilson, I. A. Vitkin, and V. X. D. Yang, Opt. Lett. **33**, 1530 (2008).
5. A. Mariampillai, M. K. K. Leung, M. Jarvi, B. A. Standish, K. Lee, B. C. Wilson, I. A. Vitkin, and V. X. D. Yang, Opt. Lett. **35**, 1257 (2010).
6. B. J. Vakoc, R. M. Lanning, J. A. Tyrell, T. P. Padera, L. A. Bartlett, T. Stylianopoulos, L. L. Munn, G. J. Tearney, D. Fukumura, R. K. Jain, and B. E. Bouma, Nat. Med. **15**, 1219 (2009).
7. T. Ju, M. L. Baker, and W. Chiu, Comput.-Aided Des. **39**, 352 (2007).
8. S. Abeysinghe, http://gorgon.wustl.edu/index.php.
9. K. Norrby, Microvasc. Res. **55**, 43 (1998).
10. M. Potente, H. Gerhardt, and P. Carmeliet, Cell **146**, 873 (2011).
11. S. Goel, D. G. Duda, L. Xu, L. L. Munn, Y. Boucher, D. Fukumura, and R. K. Jain, Physiol. Rev. **91**, 1071 (2011).
12. J. W. Baish and R. K. Jain, Cancer Res. **60**, 3683 (2000).
13. S. Lorthois and F. Cassot, J. Theor. Biol. **262**, 614 (2010).
14. J. M. Brown, J. Natl. Cancer Inst. **82**, 338 (1990).